Petr Bour[1]
Jan Kubelka[2]
Timothy A. Keiderling[2]
[1] *Institute of Organic Chemistry and Biochemistry, Academy of Sciences of the Czech Republic, Flemingovo nám. 2, 16610, Praha 6, Czech Republic*

[2] *Department of Chemistry (M/C 111), University of Illinois at Chicago, 845 W. Taylor Street, Chicago, IL 60607-7061, USA*

Received 4 April 2002; accepted 24 May 2002

Ab Initio Quantum Mechanical Models of Peptide Helices and Their Vibrational Spectra

Abstract: *Structural parameters for standard peptide helices (α, 3_{10}, 3_1 left-handed) were fully ab initio optimized for Ac–(L-Ala)$_9$–NHMe and for Ac–(L-Pro)$_9$–NHMe (poly-L-proline—PLP I and PLP II—forms), in order to better understand the relative stability and minimum energy geometries of these conformers and the dependence of the ir absorption and vibrational CD (VCD) spectra on detailed variation in these conformations. Only the 3_{10}-helical Ala-based conformation was stable in vacuum for this decaamide structure, but both Pro-based conformers minimized successfully. Inclusion of solvent effects, by use of the conductor-like screening solvent model (COSMO), enabled ab initio optimizations [at the DFT/B3LYP/SV(P) level] without any constraints for the α- and 3_{10}-helical Ala-based peptides as well as the two Pro-based peptides. The geometries obtained compare well with peptide chain torsion angles and hydrogen-bond distances found for these secondary structure types in x-ray structures of peptides and proteins. For the simulation of VCD spectra, force field and intensity response tensors were obtained ab initio for the complete Ala-based peptides in vacuum, but constrained to the COSMO optimized torsional angles, due to limitations of the solvent model. Resultant spectral patterns reproduce well many aspects of the experimental spectra and capture the differences observed for these various helical types.* © 2002 Wiley Periodicals, Inc. Biopolymers 65: 45–59, 2002

Keywords: *ab initio optimized geometry; peptide secondary structure; conformation; ir; vibrational CD*

INTRODUCTION

Helices are a dominant conformational motif of chiral periodic polymers, especially peptides. Formation of α-helices in proteins is viewed as an early stage of some protein folding processes.[1–3] Alanine-rich oligopeptides that form stable α-helical structures in solution[4] have been recognized as important models

Correspondence to: Timothy A. Keiderling; email: tak@uic.edu
Contract grant sponsor: Academy of Sciences (AS), Grant Agency of the Czech Republic (GACR), and Petroleum Research Fund
Contract grant number: A4055104 (AS) and 203/01/0031 (GACR)
Biopolymers, Vol. 65, 45–59 (2002)

for studying helix formation in proteins and have been the subject of intensive research using a wide range of experimental[5–13] as well as computer simulation techniques.[14] The balance between α-helix and 3_{10}-helix conformations has been the topic of many studies, and 3_{10}-helix formation has been recognized to be a widely occurring minor contributor to overall protein secondary structure.[15,16] In native protein structures, as revealed by x-ray crystallography, 3_{10}-helical segments are normally quite short (less than 5 residues); however, longer 3_{10}-helical segments have been observed in model oligopeptides.[15–17] Furthermore, the 3_{10}-helix has been proposed as an intermediate in the unfolding of α-helices to form random coils.[18] Poly-L-proline-(PLP)-II-like 3_1-helical structures also occur in native proteins in sequences that both do and do not contain proline residues.[19] Substantial experimental, as well as theoretical, evidence exists that this conformation is present, at least locally, in the unordered or coil states of nonproline oligopeptides.[20–27]

Various procedures have been developed for recognition of such structures in peptides and proteins based on vibrational and other spectroscopies. In particular, the vibrational CD (VCD) technique is extremely sensitive to molecular structure. A series of empirical correlations of ir frequencies and VCD (as well as electronic, uv CD) bandshapes with secondary structure are now available for proteins and peptides.[28–30] However, the most detailed interpretation of spectroscopic data is dependent on quantum mechanical computations, which are traditionally not well suited for large molecules. Thus we have attempted to develop a computational model system whose spectroscopic response is in agreement with and can be used to predict and explain experimental peptide spectra in terms of structure.

Most computational conformational analyses of oligopeptides have been carried out using empirical force field (molecular mechanics) methods. While these methods are very valuable in gaining a qualitative insight into the detailed mechanism of oligopeptide helix formation, quantitative results vary significantly depending on the specific parametrization.[31] More particularly, these methods have not yielded vibrationally accurate force fields, which have been previously obtained by empirical fits to spectral frequencies,[32] nor do they naturally encompass intensity mechanisms capable of realistic ir and VCD spectral bandshape simulations.

On the other hand, ab initio quantum mechanical simulations of spectral properties, which are vibrationally accurate and yield useful intensity information, are restricted by molecular size. Size causes problems even for the determination of the minimum energy conformation. However, many important effects can be obtained from computations on fragments of larger molecules and used to simulate some spectral properties. For instance, the major qualitative features of ir and VCD spectra of α-helical and other common peptides can be successfully simulated with just a diamide fragment.[33,34] However, such a small oligomer cannot form a stable α-helical conformation, nor would it have any other particular type of secondary structure conformation, even in vacuum, unless specific interactions between backbone and side-chain are present.[35] Furthermore, the influence on the spectra of longer-range interactions and conformational variations characteristic of a realistic nonuniform energy minimized structure could not be assessed. For computational studies on such small peptides to be useful, peptide fragments must be constrained to experimentally determined geometry parameters, in most cases taken from protein x-ray structures. But this approach has some potential disadvantages: (a) the accuracy of the x-ray (or NMR) data is often limited, (b) the structures often do not correspond to the computational local energy minimum at which well-defined properties can be calculated, and (c) the typical structural parameters for proteins may not be applicable to model oligopeptides.

Ab initio quantum mechanical calculations on peptides, reviewed recently by Császár and Perczel,[36] have focused mainly on detailed conformational properties of small peptide systems (mostly di- and triamides). Using ab initio methods that scale linearly with system size appears to be a potential alternative,[37–39] for example, a full geometry optimization with a small basis set for a 64-residue protein molecule has been reported.[40] However, current implementations of such linear methods appear to provide only molecular energies. Thus computations of spectral parameters as well as incorporation of solvent effects are still restricted to smaller systems of limited biochemical interest. In our previous approaches to this problem,[34,41,42] we have transferred parameters (geometry, force field, and intensity tensors) obtained for smaller systems to larger molecules in order to better simulate vibrational spectra as a function of structure and molecular size. Such modeling is not, in principle, restricted with respect to peptide structures and ab initio approximations, so that potentially it can be systematically improved, but it is limited in practice by finite computational capabilities. As for any approximation, testing against fully ab initio results is needed to recognize the limitations of using small molecule fragments.

The full ab initio modeling presented here naturally includes longer range forces and realistic struc-

tures as well as provides insight into the consequences of increased hydrogen bonding and the effects of Pro side chains. Solvent effects are approximated by the conductor-like screening solvent model (COSMO).[43] To the best of our knowledge, this is the first report of systematically, fully ab initio geometry optimized, sizable Ala-based oligopeptides with α-, 3_{10}-, and 3_1-helical secondary structures, along with comparable PLP I and PLP II helical optimizations, complemented by subsequent modeling of their spectroscopic properties. A study of β-sheet structures, which are in principle also helices, is not presented here because of the additional complexity associated with multiple strands. Spectral simulations of β-sheets have been the subject of independent studies (based on transfer of parameters) from our laboratory.[44–46]

METHODS

Geometry optimizations were performed with energy minimization using the Hartree–Fock (HF) and density functional (DFT) methods as incorporated in the Turbomole program package, which proved to be efficient.[47] The alanine-based decaamides, Ac–(L-Ala)$_9$–NHMe, were initialized with canonical dihedral angles[48] for α-helix, 3_{10}-helix, and 3_1(left-handed)-helix, and then fully optimized. Similarly, the proline oligopeptide, Ac–(L-Pro)$_9$–NHMe, was fully optimized starting from idealized PLP I (right-handed, *cis* amides) and PLP II (left-handed, *trans* amides) helical structures. These optimizations were attempted at both the HF and DFT/B3LYP[49] levels, using the SV and SV(P) split valence basis sets (comparable to the more common 6-31G and 6-31G* bases, respectively). Solvent effects were simulated using the COSMO model[43] default parameters in Turbomole with the exception of employing a relative permittivity of 78, appropriate for water, and using optimized atomic radii for the cavity definition.

Because of the limitations of the COSMO model, for which analytical second derivatives are not implemented in software available to us, and in order to get the results in a realizable time, spectral parameters were obtained by analytical computations only for peptides in vacuum. Thus, for the spectral simulations the entire alanine decaamides were reoptimized without solvent correction, but their torsion angles were constrained to those obtained for each of the structures when minimized with the COSMO correction. The force field (FF) and spectral intensity parameters, atomic polar and axial tensors (APT and AAT), as obtained using the magnetic field perturbation theory of Stephens,[50,51] were then calculated with the Gaussian 98 package of programs[52] at the DFT/BPW91/6-31G* level. We have used the same BPW91 functional and 6-31G* basis set[53,54] with much success in other ir and VCD spectral simulations of amide transitions for larger peptides.[44,45,55,56]

The Ac–Pro$_9$–NHMe peptide was too large for a direct ab initio frequency calculation with these methods and our current computational resources. Thus spectral parameters for three fragments, Ac–Pro$_4$–NHMe, Ac–Pro$_3$–NHMe, and Ac-Pro$_4$NHMe, constrained to torsion angles appropriate for the N-terminus, middle terminus, and C-terminus, respectively, were computed as a substitute. The Cartesian force field and intensity tensors from these smaller oligopeptides were transferred onto the appropriate residues of the larger Ac–(L-Pro)$_9$–NHMe geometry using our previously described property tensor transfer technique.[41] To get a measure of the validity of such a fragment-based spectral simulation, the same sort of calculation was made for Ala-based fragments and Ac–Ala$_9$–NHMe constrained to the 3_1-helix conformation, and the results compared to the corresponding full ab initio spectrum.

In all cases, spectral frequencies and intensities (dipole and rotational strengths) were obtained within the harmonic approximation. Vibrational spectra were simulated by assigning to each transition a Lorentzian band, with a full width at half height of 15 cm^{-1}.

RESULTS

For the Ala-based peptides, only the 3_{10}-helical structure was found to be stable with all the computational methods attempted, i.e., both in vacuum and using the COSMO solvent model, and at both the HF and DFT levels. The α-helix was stable only with the COSMO correction, both for HF and DFT, and the 3_1-helical Ala-based conformation was stable only with the HF/SV [or SV(P)]/COSMO model. In Figure 1, the 3_{10}-helical, α-helical, and 3_1-helical optimized oligopeptide conformations are compared graphically along with those of PLP I and PLP II.

3_{10}-Helix Optimized Structure

The main torsional angles (ω, φ, ψ) for both the vacuum and solvated optimized 3_{10}-helical structures obtained at the DFT/B3LYP/SV(P) level are listed in Table I along with the geometrical parameters for the hydrogen bonds associated with each amide N—H, as well as an average for the central residues. Each calculation yielded very consistent central (φ,ψ) angles, with a small (4°–5°) variance for residues 1 and 7 and much more for residues 8 and 9. The simulated solvent effects are modest, lowering φ and raising ψ by only 1°–2°, except for the terminal residues. The HF results were very similar to those shown for the DFT, (φ,ψ) being identical within about 1° and ω being slightly closer to 180°. Average (φ, ψ) angles obtained with DFT COSMO are about (−60°, −23°), which is close to the expected values of (−57°, −30°),[15] obtained from oligopeptide structures including α-Me substituted residues to obtain an "ide-

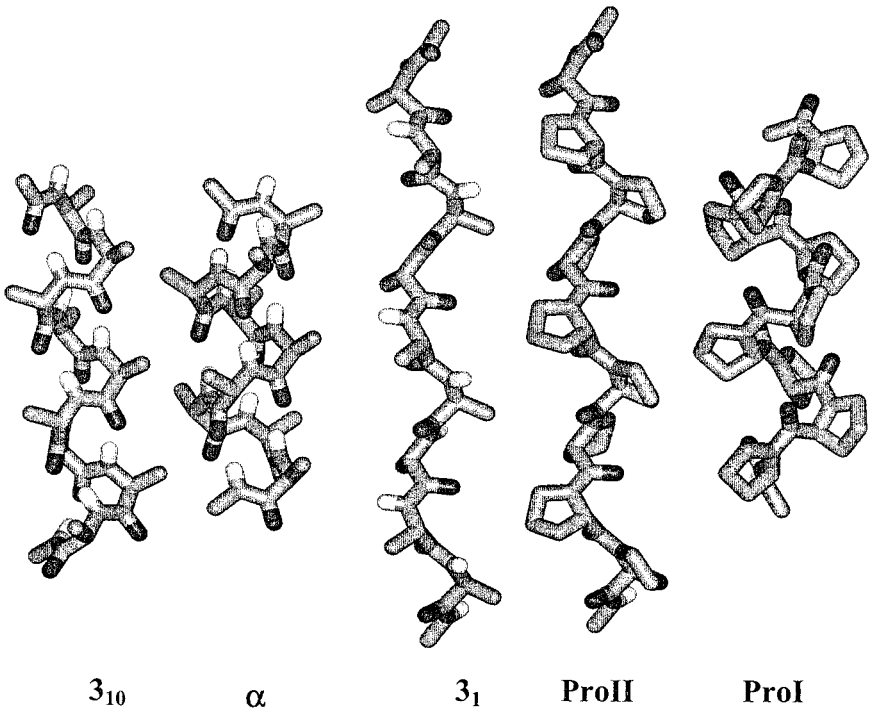

FIGURE 1 Representation of the optimized geometries for the helices used for the spectral simulations. Hydrogen atoms are displayed only for the NH group. From left to right: 3_{10}, α-, and 3_1-alanine-based helices, Ac–Ala_9–NHMe; PLP II and PLP I proline-based helices, Ac–Pro_9–NHMe.

alized" 3_{10}-helix. They are higher in φ and lower in ψ, but also approximate (especially the COSMO optimization) the experimental values obtained from the x-ray crystal structure of [L-(αMe)–Val]$_8$, a synthetic 3_{10}-helical, α-methylated octapeptide,[57] as compared in the last two columns of Table I. It might be noted that the 3_{10}-helix structure[58] used by Krimm and co-workers to empirically calculate 3_{10}-vibrations[32,59] was from older models and had a ψ value of $-45°$, which is much lower than calculated here. The ω torsional angles were computed to be slightly more planar and uniform than the experimental values. The largest deviations from planarity are observed at the N-terminus of the peptide in all calculated as well as experimental geometries.

The average N · · · O distances for hydrogen-bonded C═O · · · H—N pairs were 3.09 Å for the vacuum, and 3.01 Å in the COSMO simulated solvated state at the DFT level, and the experimentally expected value is 3.11 Å.[57] HF/SV determined values were slightly longer. The hydrogen bonds calculated in vacuum are also longer by about 0.05–0.1 Å than for COSMO, and the DFT values are about 0.05 Å shorter than for HF. The calculated —H · · · O═ distances (about 2.0–2.1 Å) are in all cases shorter than corresponding experimental values (which average about 2.27 Å).[57] The N—H · · · O angles are on average about 167° and are thus larger than the experimental values, which are scattered around 153°.[57] These values are all longer then the corresponding ones assumed in empirical FF studies.[59] It should be noted, however, that in the x-ray structural analyses H atoms were not precisely located, having been included at calculated positions by use of an idealized valence geometry.[17,57]

α-Helix Optimized Structure

The starting α-helical conformation gradually transformed to a 3_{10}-helical conformation during energy minimization in vacuum, the resulting structure being identical to that described above. With the COSMO solvent model, however, stable α-helical conformations with characteristic ($i \cdots i + 4$) hydrogen bonds were optimized at both the HF and DFT levels. The torsional angles for the (solvated) optimized α-helical structures and the respective hydrogen-bond parameters are given in Table II. As in the 3_{10} case, (φ, ψ) values for the α-helical minimized structures are more consistent in the middle of the sequence, with some distortion for residues 3 and 8 in φ, and more for

Table I Comparison of Calculated Geometry Parameters for a 3_{10}-Helix with X-Ray Data

Main-Chain Torsion Angles, in Degrees

	B3LYP/SV(P)/Vacuum			B3LYP/SV(P)/COSMO			X-Ray[a]		
Res.	ω	ϕ	ψ	ω	ϕ	ψ	ω	ϕ	ψ
N-cap	−167.4	—	—	−169.9	—	—	−172.3	—	—
1	177.8	−63.7	−25.6	178.8	−61.2	−29.0	−175.5	−56.8	−32.6
2	176.8	−58.7	−21.3	176.8	−57.9	−23.0	−173.5	−51.9	−25.1
3	176.2	−59.9	−21.6	176.8	−58.5	−24.1	−177.6	−55.6	−23.8
4	176.4	−59.9	−20.7	176.8	−58.3	−23.5	−176.3	−50.7	−30.7
5	177.4	−59.7	−21.7	176.6	−58.2	−23.4	−171.5	−50.6	−35.1
6	177.1	−59.9	−21.9	177.7	−57.7	−25.6	−168.8	−49.0	−39.4
7	176.5	−62.7	−19.8	177.2	−60.1	−23.3	−174.3	−62.2	−34.0
8	172.3	−70.3	−7.6	174.1	−66.9	−13.3	176.1	−62.5	3.0
9	178.0	−101.5⁻	9.9	180.0	−96.1	6.3			
Ave 2–7	176.7	−60.1	−21.2	177.0	−58.5	−23.8	−173.7	−53.3	−31.4

Hydrogen Bond Distances (inÅ) and angles:

	B3LYP/SV(P)/Vacuum			B3LYP/SV(P)/COSMO			X-Ray[a]		
	d	d	∠	d	d	∠	d	d	∠
Res.	N...O	H...O	N—H...O	N...O	H...O	N—H...O	N...O	H...O	N—H...O
N-cap	3.050	2.038	170.2	2.993	1.985	167.3	3.041	2.19	169.7
1	3.097	2.087	169.4	3.020	2.014	167.4	3.194	2.34	176.6
2	3.086	2.077	169.0	3.005	2.000	166.5	3.149	2.29	173.6
3	3.088	2.077	169.3	3.014	2.008	167.2	3.075	2.23	167.1
4	3.074	2.067	168.4	3.005	2.001	166.2	3.244	2.41	164.2
5	3.086	2.080	167.6	2.998	2.000	164.5	3.086	2.30	151.9
6	3.113	2.115	165.3	3.017	2.023	163.6	2.960	2.11	169.2
7	3.103	2.138	157.4	3.042	2.058	161.6	3.041	2.19	169.7
Ave 1–7	3.092	2.092	166.6	3.014	2.015	165.3	3.107	2.27	167.5

[a] From crystal structure of a 3_{10}-helical peptide, [L-(αMe)Val]$_8$.[57]

residue 9. The average (φ,ψ) angles in the center of the minimized, solvated α-helical structure are computed to be about (−63°,−42°) at the DFT level and slightly lower in φ for HF calculations. Other α-helical forms,[32,60] such as α_{II} and α_{L} have not been investigated in this study.

These results can be compared to experimental values for crystalline α-helical polyalanine peptides[61] as well as to crystal coordinates for a large number of α-helices from protein structures. However, we are unaware of any precise experimental structures for short α-helical alanine oligopeptides. For a comparative data set, we arbitrarily chose the highly uniform C-helix (residues 88–100) of hen egg white lysozyme (HEWL), whose structure was solved to 1.33 Å resolution[62] (PDB code 193L) and which seems to be a suitable length for comparison with our optimized geometry parameters. Corresponding torsional angles and hydrogen bond parameters for the HEWL C-helix are listed in Table II. Our computed values are clearly in better agreement with those for the HEWL fragment (−63°,−43°), than are the accepted polypeptide values reported for the x-ray structure of regular polyalanine helices (−57°,−47°).[61] Unlike for the solvated 3_{10}-helix case, the computed α-helical hydrogen-bond lengths are not shorter than the experimental values, but are even slightly longer. However, aside from the N-cap, the N · · · O distances average ~3.0 Å, a reasonable match to these experimental values which vary quite a bit. Values from HF calculations are even longer (~3.1 Å). The amino group at the N-terminus of the helix participates in a bifurcated

Table II Calculated Torsional Angles and Hydrogen Bond N…O Distances for the α-Helix as Compared with X-Ray Parameters

B3LYP/SV(P)/COSMO					X-Ray[a]				
Res.	ω	ϕ	ψ	d(N…O)	Res.	ω	ϕ	ψ	d(N…O)
N-cap[b]				3.121					
N-cap	−172.2	—	—	3.121	88	−178.8	—	—	2.916
1	−179.1	−58.3	−38.6	2.965	89	−178.3	−45.9	−50.5	3.017
2	177.5	−63.4	−38.1	3.032	90	179.4	−63.1	−44.1	3.493
3	175.9	−67.3	−42.2	2.977	91	180.0	−60.4	−44.2	2.942
4	178.8	−60.1	−44.0	2.990	92	180.0	−65.5	−46.8	2.842
5	178.6	−61.8	−44.7	2.966	93	179.3	−60.1	−40.7	3.006
6	179.2	−60.8	−43.6	2.935	94	179.3	−71.0	−40.2	2.874
7	−179.8	−63.0	−41.2		95	178.7	−59.6	−36.6	2.885
8	−177.2	−68.4	−39.4		96	179.6	−61.6	−39.9	3.327
9	−176.4	−78.7	−31.4		97	178.0	−69.2	−41.8	3.233‡
Ave 2–7	178.4	−62.7	−42.3			179.5	−63.3	−42.1	3.007

[a] Taken from the crystal structure of HEWL,[62] PDB code 193L; C-helix, res. 88–100.
[b] (*i*, *i*+3) hydrogen bonds.

H-bond, one of a 3_{10}-helical ($i \cdots i + 3$) and the other of an α-helical ($i \cdots i + 4$) type, which results in added stabilization of the helix.

3_1-Helix (Left-Handed) and PLP II and PLP I Helices

The left-handed 3_1-helical Ala-based decaamide structure was stable during the optimization only if the COSMO solvent model was included, and then, in our hands, only at the HF level. With other computational methods the molecule optimized to an irregular shape having segments of extended conformation [all torsion angles (φ,ψ,ω) close to 180°]. On the other hand, the Ac–(L-Pro)$_9$–NHMe structure did successfully optimize for both the PLP II and PLP I conformations, at both the HF and DFT levels with COSMO. The (ω,φ,ψ) angles for the left-handed 3_1-helical Ac–Ala$_9$–NHMe and PLP II (*trans* amides) are given in Table III. The results for PLP I, right-hand helical with *cis* amides, are in Table IV. The Ala-based 3_1-helix, when optimized at the HF level, gave (φ,ψ) values that averaged (−68°,152°), which are indeed very similar to those of the PLP II helix (DFT level), which averaged (−70°,158°), confirming that the left-handed 3_1-helix is a general peptide conformation, even if the potential well may not be deep for L-Ala residues. For PLP II, the HF-determined (φ,ψ) values were somewhat smaller, averaging (−68°,152°), almost identical to the HF values for Ac–Ala$_9$–NHMe.

For comparison to an experimental oligoproline structure, the torsional angles of an L-proline octamer obtained from the x-ray structure of the profilin–poly-L-proline complex are given in Table III.[63] The overall agreement of our predicted (φ,ψ) values with the experimental average (−69°,160°) is very good. The optimized (φ,ψ) for both the PLP II and Ala-based 3_1-helices are in only very rough agreement with the values used for empirical normal mode analysis of polyGly II (−77°,145°), which is also 3_1-helical.[32,64] These latter values do reflect those that had been taken as a standard for poly-L-proline II (−78°, 149°). Amide groups in the computed PLP I and PLP II conformations are less planar (distorted by ∼13° and 9°) than those for the computed α- and 3_{10}-helical cases; the same is true for the Ala 3_1-helix at the HF/COSMO level. This deviation of ω from 180° for the computed PLP II helices is much more than is found experimentally and correlates to a slight pyramidal configuration of the amide nitrogens.

Energy and Electrostatic Field

The relative conformer energies are summarized in Table V. These values are not corrected for the vibrational energy, which should not significantly affect the relative energies due to their structural similarity. For the alanine-based decamer the energy of the 3_{10}-helical structure is slightly higher than for the α-helix, by 5.5 and 3.4 kcal/mol for the HF and DFT calculations, respectively. For the Ala-based 3_1-helix, the

Table III Calculated Main Torsional Angles for Ala-II and Pro-Based Oligomers in the 3_1-Helical Conformation, Comparison with X-Ray Data

	Ac–Ala_9–NHMe[a]			Ac–Pro_9–NHMe[b]			X-Ray[c]		
Res.	ω	φ	ψ	ω	φ	ψ	ω	ϕ	ψ
N-cap	175.9	—	—	178.5					
1	171.6	−69.8	153.8	170.6	−71.0	156.0	−179.5	112.2	80.3
2	174.3	−66.7	152.5	171.8	−70.0	157.5	179.8	−62.8	164.5
3	172.2	−66.5	148.5	170.6	−69.9	157.0	180.0	−76.8	157.5
4	172.2	−70.0	154.1	170.4	−70.4	158.4	180.0	−60.7	133.6
5	173.5	−67.1	151.3	172.3	−68.7	156.5	179.6	−75.6	166.9
6	171.6	−68.8	151.0	170.4	−70.8	156.8	180.0	−63.4	160.5
7	172.5	−69.8	154.5	170.4	−70.4	159.1	179.4	−72.8	176.3
8	173.1	−67.5	150.8	172.8	−68.7	156.1	180.0	−75.4	157.8
9	176.4	−68.5	149.7	176.8	−70.0	152.1	−179.3	−49.7	158.6
Ave 2–7	172.7	−68.2	152.0	171.0	−70.0	157.6	179.8	−68.7	159.9

[a] HF/COSMO/SV.
[b] B3LYP/COSMO/SV(P).
[c] Profilin-poly-L-Pro complex,[63] PDB code 1AWI.

carbonyls would be fully hydrogen bonded to the solvent in H_2O, which cannot be adequately modeled by just the COSMO model.[65] For other nonspecifically interacting solvents, this model may provide a better estimate, and the results are consistent with the propensity of the Ala oligomers (if soluble) to form α-helices in nonpolar solvents. The relative energy of the 3_1-helix (HF only) thus appears to differ from that of the α-helix by the rather high value of 26.8 kcal/mol since the 3_1 structure lacks any H-bond stabilization in this comparison, while the α- and 3_{10}-helices have internal H-bonds. For Ac–Pro_9–NHMe, the DFT/COSMO level calculations predict a much lower energy difference between the PLP I and PLP II conformations than do the HF results.

Calculated dipole moments are compared in Table VI. For the 3_1- and PLP II helices, the amide group dipole moments are oriented almost perpendicular to the helical axis resulting in a small net dipole moment (less so for Pro than Ala, presumably due to the predicted amide nonplanarity). On the other hand, the more in-phase dipole moment orientations in the α- and 3_{10}-helices result in a large net molecular moments for these conformations, the α-helical dipole being about 10% larger than the 3_{10}-helical dipole. Since the dipole moment for N-methyl-acetamide (NMA) calculated at the B3LYP/SV(P)/COSMO

Table IV Calculated Main Torsional Angles for L-CH_3–Pro_9–NHMe, PLP I Conformer

	B3LYP/SV(P)/COSMO		
Res.	ω	φ	ψ
N-cap	−2.5		
1	−12.6	−83.5	158.4
2	−10.2	−76.8	160.5
3	−13.1	−74.3	164.6
4	−13.5	−71.7	165.6
5	−12.4	−71.6	165.3
6	−13.2	−72.2	166.2
7	−13.5	−71.7	166.9
8	−10.9	−69.5	166.1
9	−5.5	−68.1	164.6
Ave 2–7	−12.7	−73.1	164.9

Table V Calculated Relative Energies for the Optimized Peptide Structures[a]

Structure Type	HF/SV	HF/SV/COSMO	B3LYP/SV(P)/COSMO
Ac–Ala_9–NHMe			
3_{10}-Helix[a]	0	0	0
α-Helix	—	−5.5	−3.4
3_1-Helix	—	21.3	—
Ac–Pro_9–NHMe			
PLP II	0	0	0
PLP I	13.8	29.8	3.3

[a] All energies in kcal/mol.

Table VI Calculated Dipole Moments for Optimized Peptide Structures

	$\|\mu\|$ (Debye)	μ_z[a](Debye)
Alanine-like structures		
α-Helix[b]	48.6	48.5
3_{10}-Helix[b]	43.5	43.4
3_1-Helix[c]	5.6	−4.1
Proline polymers		
PLP I[b]	49.4	−49.3
PLP II (3_1-helix)[b]	12.2	−11.5

[a] Projection to the helical axis from C to N-terminus.
[b] B3LYP/SV(P)/COSMO.
[c] HF/SV/COSMO.

level is 5.05 Debyes, and oriented 165° from the C═O, we can vectorially sum up what might have been expected for ten aligned NMA-like dipoles in the α- and 3_{10}-helical conformations. We obtain 43.2 Debyes for the α-helix and 38.7 Debyes for the 3_{10}-helix, the difference (4.5 Debyes) being about the same as we calculated directly for the entire peptide (5.1 Debyes), which is due to the more favorable alignment in the α-helix conformation. The difference (~10%) between these sums and the computed values (Table VI) may be due to helix polarization or to errors in using NMA to approximate the amide contribution to the dipole moment of an oligopeptide.

VCD and Absorption Spectra

Simulated VCD and absorption spectra of the alanine decamer in the α-, 3_{10}- and 3_1-helical conformations are plotted in Figure 2 for both the N-deuterated and N-protonated forms. N-deuterated peptide isomers in D_2O are often measured in order to avoid overlap with water absorption bands, so the comparison of these isotopic variants is experimentally useful. These simulations were obtained with fully ab initio calculations but were done at the DFT/BPW91/6-31G* level, re-optimized with all backbone torsions frozen to the COSMO results. Thus we have the solvent-stabilized conformation with all local coordinates relaxed for better computational stability for the high frequency modes. The frequency range shown in the figures includes the most studied experimentally accessible regions of the amide I and II vibrations as well as a part of the lower-frequency region consisting of the amide III modes mixed with $^{\alpha}$C—H deformations and with peptide backbone vibrations. For most peptides and proteins, little beyond this range has been measured, and thus we cannot usefully compare all the other computed modes with experimental data.

The simulations correctly predict the main features of the observed spectra. The ir bands reflect our experience in computing amide vibrational transitions with DFT. The amide I is predicted rather too high and the amide II a little low in frequency resulting in an amide I–II splitting much larger than seen experimentally. The individual components of the α- and 3_{10}-helical amide I and II bands are each quite dispersed (40–50 cm^{-1}), but most of the intensity is transferred to just a few of them, resulting in a narrower bandshape. The frequency difference between the α-helix and 3_{10}-helix amide I results from the most intense 3_{10}-helical transition being nearly the lowest component of the exciton split band (~35 cm^{-1} dispersion), while that for the α-helix is in the middle of its dispersion. Both the bands also develop side band components that correlate to different (incomplete) H-bonding patterns.[44–46] In these simula-

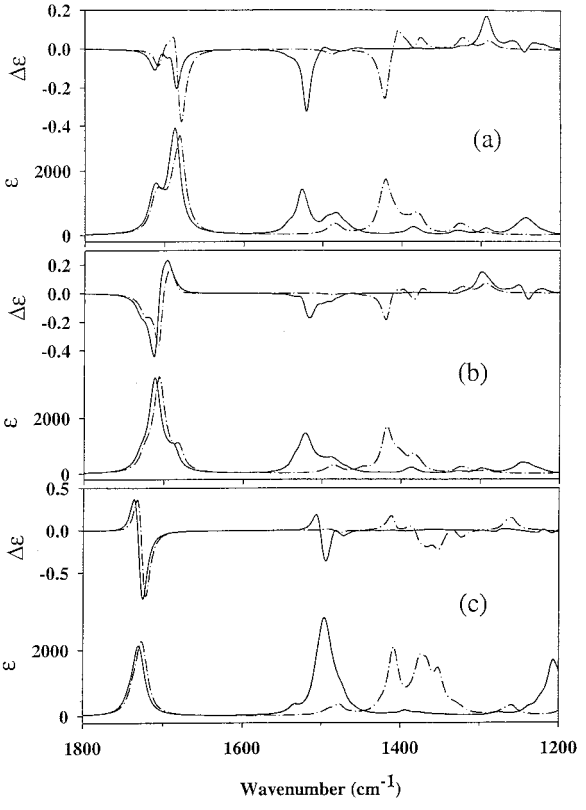

FIGURE 2 Fully ab initio simulated VCD and absorption spectra of Ac–$(Ala)_9$–NHMe over the amide I–III regions for the three optimized helical conformations (as stabilized by the COSMO simulated solvent effect) and their response to N-deuteration. N-protonated (solid line) and N-deuterated (dash-dot line) spectra for (a) 3_{10}-helix, (b) α-helix, and (c) 3_1-helix conformations.

tions, the side-chain C—H deformations partially mix with the amide II forming the broad feature predicted at ~1480 cm^{-1}, thereby distorting the amide II shape more than is seen experimentally, where the separation of these modes is clearer. Since there is no H-bonding in the 3_1-helix model, the amide I is higher and amide II lower than for the 3_{10}- and α-helical results, which encompass several internal H-bonds. For all the conformations, N-deuteration causes a small downshift of the amide I frequencies and a more significant (~100 cm^{-1}) change for the amide II, both as expected. The relative intensity of the amide I–III modes is qualitatively reasonable, but experimentally the I:II ratio is closer to 1.5, while for the α- and 3_{10}-helices a larger ratio is predicted and for the 3_1-helix a much smaller value (<1) is simulated. In this latter case, we have shown that addition of explicit solvent (H_2O) to the calculation will result in a more realistic intensity ratio.[56] The amide III is very weak and is dispersed over a number of transitions mixed with $^{\alpha}$C—H deformations.

The VCD of the α-helical amide I is predicted to have a distinct positive couplet that is negatively biased, in agreement with all of our previous α-helix calculations, and a broad negative amide II whose negative extremum is lower by 5 cm^{-1} in frequency than the absorbance maximum, in qualitative agreement with the experimental results. The weak positive VCD features in the amide III are dispersed much as is the absorbance. The 3_{10}-helix has much weaker amide I VCD and stronger negative amide II VCD, in accordance with experiment. However, for the 3_{10}-helix amide I, a third negative band is predicted to lie on the low frequency side of the absorbance maximum in the N-protonated species and actually dominates the predicted N-deuterated 3_{10}-helical VCD. Computationally, the difference in the 3_{10}- and α-helix VCD pattern arises from the relative position of the most intense transition (polarized along the helix axis), which in both cases has negative VCD. However, for the α-helix this transition is higher in frequency than a positive VCD component, and for the 3_{10}-helix lower. This most-intense component originates in an in-phase C═O stretching vibration of the central amide groups.

The sign of the amide I couplet switches for the left-handed 3_1-helix VCD and its absolute intensity increases, both of which are in excellent agreement with data for peptides thought to have local 3_1-helical structure (random coil peptides) and with the intense VCD of PLP II.[22,66,67] The amide II VCD becomes more complex, having a negative couplet pattern with the negative component to the low frequency side of the absorbance, which is in qualitative agreement with experiment, aside from frequencies. The VCD sign pattern is generally preserved through spectral shifts accompanying deuteration, although the amide II bandshape is distorted by mixing with the C—H deformation modes.

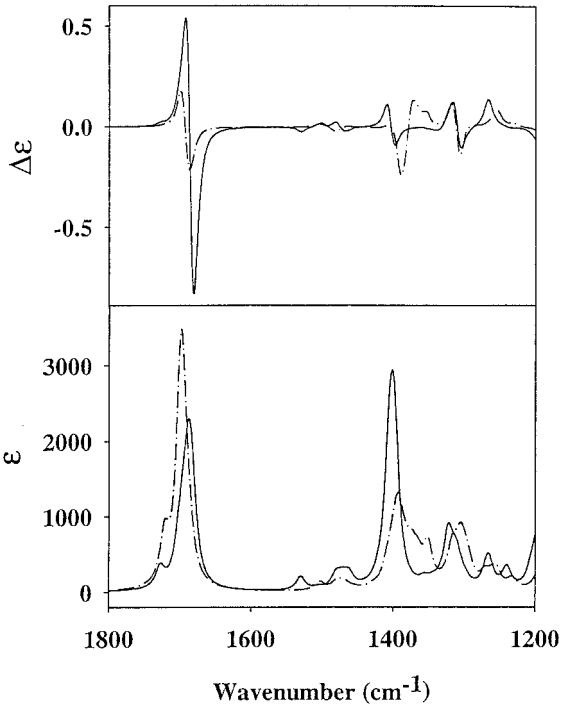

FIGURE 3 Simulated amide I–III absorption and VCD spectra of Ac–$(Pro)_9$–NHMe in the optimized PLP I (dash–dot line) and PLP II (solid line) conformations, as obtained by transfer of spectral parameters from three fragments as described in the Methods section.

Since we cannot at this point compute ab initio frequencies for the entire Ac–Pro_9–NHMe oligopeptide, the PLP I and PLP II spectra were simulated using ab initio parameters calculated for fragments and transferred to the target peptide, the results of which are compared in Figure 3. The two conformations have some distinct spectral differences. The PLP I amide I absorbance is here predicted to be slightly higher in frequency and more intense than that of the PLP II, and they have the opposite intensity relationship in VCD. Both computations predict a negative amide I VCD couplet, though the helices have the opposite sense, which is presumably an effect of *cis* (PLP I) vs *trans* (PLP II) amide bonding on the chiral sense of amide interactions in each helix. The intense ir mode at 1400 cm^{-1} is primarily due to the C—N stretching motion and has couplet VCD band shape of the opposite sense for the two forms. Our Fourier transform infrared (FTIR) data for PLP II in D_2O

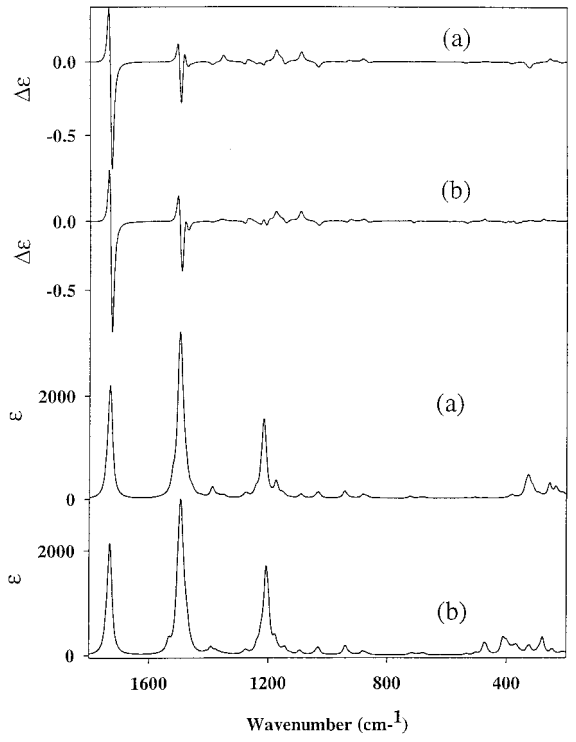

FIGURE 4 Absorption and VCD spectra of Ac–Ala_9–NHMe in the (HF/COSMO) optimized 3_1-helical conformation over an extended spectral region as obtained by (a) transfer from fragments and (b) full ab initio calculations.

indicate a moderate intensity band at $\sim$1460 cm^{-1} and another weaker mode at $\sim$1330 cm^{-1}, which agrees with the Figure 3 (solid line) PLP II prediction, aside from detailed intensities. Overall the amide I VCD results are in excellent agreement with experiment, matching both sign patterns and relative intensities[21,66,67]; however, the lower energy modes have not been yet studied. On the other hand, the relative PLP I and PLP II amide I frequencies are experimentally very solvent dependent, agreeing with this predicted ordering in water but evidencing the opposite order in less polar solvents.[66,68]

To test the fragmentation method, the same approach was used for the Ac–Ala_9–NHMe in a 3_1-helix, and the results are compared to the full ab initio simulation in Figure 4. Clearly, the agreement in both absorbance and VCD for the amide I and II modes is nearly perfect. The only significant difference in the computed bandshapes between the fragment and fully ab initio method is for the modes below 600 cm^{-1}, which we have included in Figure 4, even though there is no comparative experimental data for these transitions. This strongly argues that the fragmentation approximation used to simulate the Ac–Pro_9–NHMe spectra should have a negligible effect on the important aspects of the VCD and absorption spectra for the high frequency, localized amide modes normally studied in peptides.

DISCUSSION

Structural Optimization

These computed structures form a relatively accurate set of energy-minimized conformations for a simple pseudodecamer. Use of structural parameters from such minimum energy geometries have let us develop ab initio theoretical force fields in a consistent manner and thereby model Raman, ir absorption, and VCD spectra. Similar models for shorter oligopeptides, which were minimized while constrained to ideal model or experimental helical torsional angles, have been published separately.[27,34] In addition, interesting lessons with regard to the details of structure stabilization and the relative energetics of short (from the experimental point of view) helical alanine homooligopeptides can be learned from these optimization calculations. In terms of structural parameters, we have focused mainly on torsional angles and hydrogen bonds, because these are most important aspects of the structure for the questions we raise. Bond lengths and angles are more dependent on the details of the calculational method in ways that have been explored by others with higher precision for small molecules.[36,69] Here our goal is to describe peptide conformation essentially in terms of (φ,ψ) and H-bond geometry.

As demonstrated above, the inclusion of the solvent, even with a relatively simple continuum model, seems to be necessary for obtaining energy-minimized conventional helical peptide structures with these theoretical methods. While the 3_{10}-helical structure was stabilized in vacuum for this Ac–Ala_9–NHMe oligopeptide, a stable energy minimum was not found in vacuum for either the α- or 3_1-helix. Both the 3_{10}- and α-helical structure in vacuum converged to the same, 3_{10}-helical conformation. On the other hand, with a solvent correction (COSMO), the α-helical structure of this peptide does converge to an energy minimum and is, in fact, even more stable (apparently by 3–4 kcal/mol) than its 3_{10}-helical structure. Qualitatively, the latter result is in agreement with a number of studies on the relative α- vs 3_{10}-helix stability,[70–72] and even quantitatively falls in the expected range for α–3_{10} relative energies (0.6–1.6 kcal/mol) as proposed by Young and Brooks using empirical force fields.[73] The third helical type, 3_1- or PLP II-like helix, was also found to have a stable local

energy minimum with the continuum solvent model at the HF level; however, this minimum is at a significantly higher energy than that for the α- and 3_{10}-helices. The lack of a stable 3_1-helix minimum for the Ala-based peptide at the DFT/COSMO level with the default parameters that succeeded for the other helices is surprising. That the 3_1-structure shifts to a more extended form suggests that the potential well containing the 3_1-conformation is quite shallow. The 3_1-helix is not stabilized by internal hydrogen bonds, and the resulting stabilization that would be provided by specific interactions with the solvent could not be included, even in the COSMO model. By contrast, with the conformational constraints provided by the bridging pyrrolidine side chain in L-Pro, the PLP II helix converged very rapidly to the same 3_1 conformation and was significantly more stable than the PLP I helix. This apparent ease of convergence is consistent with the experimental stability of the PLP II helical form for Pro oligomers.[66,68,74]

In α- and 3_{10}-helices the polar groups are favorably oriented along helical axes, giving rise to large net dipole moments. The larger dipole moment of the α-helix is due to its more parallel orientation of amide C═O and N—H groups (Figure 1) and denser spatial distribution of the polar amide groups in the wider and shorter α-helix as compared to the more extended 3_{10}-helical structure. The strong α-helical dipole moment has been recognized for its importance in protein tertiary structure and overall function—namely, for its stabilizing effect in packing of α-helices.[75,76] The dipole moment of a PLP II-like 3_1-helical structure, on the other hand, is much smaller (an order of magnitude less) because the polar groups are approximately normal to the helical axis, which tends to cancel their mutual contributions, and offers no stability enhancement for an isolated molecule.

The effect of the solvent (within the COSMO approximation) can be examined by comparing the vacuum and solvated minimum energy 3_{10}-helical conformations. The presence of a polarized continuum surrounding the molecule leads to a slight shortening of the hydrogen bonds ($<$0.1 Å). The change, however, is somewhat dependent on the choice of the atomic radii parameters in the COSMO model. Nevertheless, the shortening is consistent with the concept of enhancing the polarity of the hydrogen bonds by the solvent, making them shorter and therefore stronger. This, perhaps nonintuitive, result may computationally explain why the α-helical structure was stable in the COSMO model solvent, since the hydrogen bonds, as one of the main stabilizing factors of the peptide helix, are strengthened in comparison to vacuum. In the COSMO corrected calculations, all the C═O bonds in the peptide were also found to be slightly longer (by about 0.005 Å). It is important to recognize that the COSMO model cannot adequately model specific solvent interactions, such as occur in aqueous solutions, as we have previously shown for N-methyl acetamide.[65]

For the Ala-based 3_1-helix, rather than strengthening the hydrogen bonds, the continuum polarization stabilized non-hydrogen-bonded C═O and N—H dipoles. The lack of hydrogen bonds correlates to shorter C═O (on average ~1.217 Å in the 3_1-helix, while ~1.229 and 1.230 Å in α- and 3_{10}-helix, respectively) and N—H bonds (~1.017 Å in 3_1-, ~1.022 Å in α- and 3_{10}-helices). For a real, aqueous peptide, the H_2O solvent will compete with internal groups to hydrogen bond to the amide groups. In a 3_1-helix, the C═O groups are well exposed to the solvent, which in water leads to solvent H-bond stabilization. This solvation effect is probably why the 3_1 extended helix is a structural form that is similar to that often proposed for aqueous "random coil" polypeptides[21,24,25] and in loop structures in proteins.[19] Since our calculations do not include explicit water, they cannot fully account for such stabilization.

In the α-helical case, the ends of the helix were computed to be slightly irregular as can be seen both from torsional angle variation as well as development of bifurcated hydrogen bonds corresponding to both α- and 3_{10}-helix-like contacts. Such irregularities and capping effects at the ends of α-helices are expected for short peptides[77] and are quite common in proteins,[78] even though these latter often include side- to main-chain hydrogen bonding or hydrophobic interactions. Bifurcated H-bonds, especially at the C-terminus, where one C═O becomes an acceptor of more than one N—H, are frequently observed,[78] and can be seen in the HEWL C-helix we used for comparison. Bifurcation of the H-bond is aided by some distortion of (φ,ψ) allowing the amide group to tilt. Side-chain interactions usually dominate the N-terminal helix capping, as the side chains for L-amino acids are oriented toward the N-terminus,[78,79] but these are not an issue with our model alanine-based sequences. Side-chain interactions can lead to some of the known sequence dependencies for helix propagation and termination in protein structures.

Vibrational Spectra

As expected from our previous work on idealized helical structures, the computed frequencies of the amide bands deviated from experimental values.[27,34,42,44,65] The amide I is systematically much too high in frequency and the amide II is low and

split. This again is a result of hydrogen bonding. Free amide residues generally contribute to the low branch of the amide II and to the high shoulder of the amide I. Hydrogen bonding to the solvent can have a different and more complex effect on the structure and vibrations. This is partially evident in the significant frequency shift between amide I and II frequencies for the α- and 3_{10}-helices and those for the 3_1-helix (Figure 2) that are higher and lower, respectively, due to the lack of any H-bonds. Amide I vibrational frequencies (mainly C═O stretch) for peptides in vacuum are routinely computed to be about 100 cm^{-1} higher than experimentally observed for even nonaqueous solution phase peptides.[65] Longer and therefore weaker C═O bonds together with stronger H-bonds to the oxygen, as we have obtained with COSMO, would shift the amide I vibrational frequencies to lower wavenumbers and thus closer to the experimental values. Of course, these effects are not evident in these decaamide spectral simulations since we unfortunately could not implement COSMO for FF determination on such large systems with our current capabilities. We have, however, previously demonstrated such effects for NMA both with and without explicit waters of solvation. Furthermore, the known difference between the amide I vibrational frequencies for helices in proteins ($\sim$1650 cm^{-1}) and short peptides, which are fully solvated in D_2O ($\sim$1635 cm^{-1}) has often been termed a "solvated helix" effect. Added H-bonds to the solvent and the higher dielectric constant of water as compared to the protein interior could reduce the C═O bond strength and thereby lower the frequency.

Predicted H/D exchange shifts of a few cm^{-1} for the amide I and $\sim$100 cm^{-1} for the amide II reflect experiment. These calculations also qualitatively reproduced the changes in VCD spectra during the PLP I/PLP II mutarotation observed for polyproline structures.[66] Finally, in a test of using the transfer method for obtaining ir and VCD simulations from fragments for the Ala-based 3_1-helix (Figure 4), the patterns obtained fully match the ab initio results except at very low frequencies. The low-frequency modes are presumably affected most by fixing the torsion angles in the fragments. Furthermore, comparison of the PLP II results (Figure 3) to the 3_1-helical (Figures 2 and 4) Ac–Ala_9–NHMe results shows they only differ in the apparent amide I frequency, a difference that arises due to the tertiary amides in PLP II. Since no hydrogen bonds are present for this model and the C═O groups are normal to the helical axis, the long-range interaction seems to be dramatically reduced, making the fragment method more applicable. This is in agreement with the previous observation of VCD arising from short-range interactions.[21,33]

The intensities of the vibrational spectra for the main amide features agree with the experiment (with the exception of the Ala-based 3_1-helical amide II ir being too intense). It was not possible to simulate the influence of the solvent on spectral intensities for these decaamide oligopeptides. However, on the basis of our experimental experience and our recent theoretical tests on small solvated peptides,[23,34,56,65] the patterns we calculate without solvent are generally relevant. VCD poses a strong test of the normal mode character, sampling both the intensity parameters and the orientation of the transition moments. The simulated amide I VCD spectra of α- and 3_1-helices are in near quantitative agreement with experimental spectral band shapes for model systems. These α- and 3_1-helix results follow the same patterns obtained in previous simulations of peptide spectra based on ab initio simulations for small fragments and their transfer to larger systems.[27,42] The comparisons in Figure 4 show the 3_1-helical result to be virtually immune to the fragmentation method, exactly following the ab initio result except for the low energy modes. However, for other structures (α- and 3_{10}-helix) such a comparison is more complex due to the difference in the fraction of residues involved in internal H-bonding between the fragments and the full helix. This problem has led us to use 7-peptide and 5-peptide fragments (which provide a fully H-bonded central amide group) to model extended α- and 3_{10}-helices, respectively.[34] The amide II does show more variations with the computational model used, but the general characteristics are present and agree qualitatively with experiment. The close agreement of the amide I VCD for the Ala-based 3_1-helix (Figure 2, fully ab initio) and the PLP II helix (Figure 3, by transfer) is especially satisfying and demonstrates the independence of the amide VCD from side chains. These computations also are in qualitative agreement with results computed for Gly oligomers,[33,55] which further demonstrates their independence from the nature of the side chains. The exception to this arises if Pro residues are mixed with normal secondary amides in the peptide chain. Then the tertiary amide will be a singularity, its amide I occurring at lower frequency and its amide II missing.[46,56]

The behavior of the amide I band in the 3_{10}-helix is somewhat surprising. Previous calculations with small peptides predicted a weak negative or a weak positive couplet amide I VCD and a very strong negative amide II. The calculations presented here have a negative W-shaped band evidencing a negative couplet component when deuterated. Experimentally

such a low-frequency negative signal can be seen if the peptide has substantial Ala content.[56] This is not seen for peptides of mostly α-Me-substituted residues and is not calculated for Aib-containing 3_{10}-helices.[55] This difference is presumably due to mixing of the amide I with the $^{\alpha}$C—H deformation, which cannot happen in α-Me residues. This low-lying negative band in the 3_{10}-helical amide I corresponds to the maximally ir intense, helical axis polarized transition. In the α-helix this component is in the center of the band, but in the 3_{10} model it moves down to the low frequency edge of the exciton band. The amides in the 3_{10}-helix deviate more from the helix axis than in the α-helix, leading to smaller net dipole moment (Table VI), which may also couple more perpendicular component into the 3_{10} transition, but we have no clear explanation for this response and its difference from experiment. In α-helices such a low-frequency negative component is commonly seen experimentally for N-deuterated peptides.[30,80] Comparative 3_{10}- and α-helix simulations have shown that both yield positive couplet amide I VCD with our transfer methods using parameters from 5-peptide and 7-peptide fragments, respectively.[55] Model calculations, using parameters transferred from much longer helices, have suggested such a component, but with much less intensity.[56] This issue requires added study to explain.

CONCLUSIONS

With COSMO, stable α-, 3_{10}- and 3_1-helical structures were obtained for the model decaamide that provided geometry parameters and vibrational spectral intensities analogous to those found experimentally for these structures. The polarized continuum stabilizes hydrogen bonds (in the α- and 3_{10}-helices), as well as nonhydrogen-bonded amides (in the 3_1-helix). In vacuum, the only stable helical structure we found was the 3_{10}-helix, while in simulated solvent the α-helix is energetically slightly more favorable. Structural parameters obtained for solvated oligopeptides agree with those known from x-ray structures for native-state proteins and peptide models, although in a sense they are unique, since no structures of short oligoalanine peptides are available. Simulated absorption and VCD spectra are in a good agreement with experimental data for these peptide helices.

This work was supported by the Grant Agency of the Academy of Sciences (A4055104 to PB), Grant Agency of the Czech Republic (grant 203/01/0031 to PB), and by a grant from the donors of the Petroleum Research Fund, administered by the American Chemical Society (to TAK).

REFERENCES

1. Baldwin, R. L. TIBS 1989, 14, 291–294.
2. Levitt, M.; Gerstein, M.; Huang, E.; Subbiah, S.; Tsai, J. Ann Rev Biochem 1997, 66, 549–579.
3. Dobson, C. M.; Sali, A.; Karplus, M. Angew Chem (Int Ed in English) 1998, 37, 868–893.
4. Marqusee, S.; Robbins, V. H.; Baldwin, R. L. Proc Natl Acad Sci USA 1989, 86, 5286–5290.
5. Dyson, H. J.; Wright, P. E. Ann Rev Biophys Biophys Chem 1991, 20, 519–538.
6. Scholtz, J. M.; Baldwin, R. L. Ann Rev Biophys Biomol Struct 1992, 21, 95–118.
7. Miick, S. M.; Casteel, K. M.; Millhauser, G. L. Biochemistry 1993, 32, 8014–8021.
8. Anderegg, R. J.; Wagner, D. S.; Stevenson, C. L.; Borchardt, R. T. J. Amer Soc Mass Spectrometry 1994, 5, 425–433.
9. Williams, S.; Causgrove, T. P.; Gilmanshin, R.; Fang, K. S.; Callender, R. H.; Woodruff, W. H.; Dyer, R. B. Biochemistry 1996, 35, 691–697.
10. Thompson, P. A.; Eaton, W. A.; Hofrichter, J. Biochemistry 1997, 36, 9200–9210.
11. Yoder, G.; Polese, A.; Silva, R. A. G. D.; Formaggio, F.; Crisma, M.; Broxterman, Q. B.; Kamphuis, J.; Toniolo, C.; Keiderling, T. A. J Am Chem Soc 1997, 119, 10278–10285.
12. Hudgins, R. R.; Jarrold, M. F. J Am Chem Soc 1999, 121, 3494–3501.
13. Lednev, I. K.; Karnoup, A. S.; Sparrow, M. C.; Asher, S. A. J Am Chem Soc 1999, 121, 8074–8086.
14. Brooks, C. L., III; Case, D. A. Chem Rev 1993, 93, 2487–2502.
15. Toniolo, C.; Benedetti, E. Trends Biol Sci 1991, 16, 350.
16. Bolin, K. A.; Millhauser, G. L. Acc Chem Res 1999, 32, 1027–1033.
17. Gratias, R.; Konat, R.; Kessler, H.; Crisma, M.; Valle, G.; Polese, A.; Formaggio, F.; Toniolo, C.; Broxterman, Q. B.; Kamphuis, J. J Am Chem Soc 1998, 120, 4763–4770.
18. Millhauser, G. L. Biochemistry 1995, 34, 3873–3877.
19. Stapley, B. J.; Trevor, P. C. Protein Sci 1997, 8, 587–595.
20. Tiffany, M. L.; Krimm, S. Biopolymers 1968, 6, 1379–1382.
21. Dukor, R. K.; Keiderling, T. A. Biopolymers 1991, 31, 1747–1761.
22. Keiderling, T. A.; Silva, R. A. G. D.; Yoder, G.; Dukor, R., K. Bioorg Med Chem 1999, 7, 133–141.
23. Keiderling, T. A.; Xu, Q. Adv Protein Chem 2002, in press.
24. Paterlini, M. G.; Freedman, T. B.; Nafie, L. A. Biopolymers 1986, 25, 1751–1765.
25. Woody, R. W. Adv Biophys Chem 1992, 2, 37–79.
26. Park, S.-H.; Shalongo, W.; Stellwagen, E. Protein Sci 1997, 6, 1694–1700.

27. Silva, R. A. G. D.; Kubelka, J.; Decatur, S. M.; Bour, P.; Keiderling, T. A. Proc Natl Acad Sci U S A 2000, 97, 8318–8323.
28. Surewicz, W.; Mantsch, H. H.; Chapman, D. Biochemistry 1993, 32, 389–394.
29. Venyaminov, S. Y.; Yang, J. T. In Circular Dichroism and the Conformational Analysis of Biomolecules; Fasman, G. D., Ed.; Plenum Press: New York, 1996; pp 69–107.
30. Keiderling, T. A. Circular Dichroism: Principles and Applications, 2nd ed.; Berova, N., Nakanishi, K., Woody, R. W., Eds.; Wiley: New York, 2000; pp 621–666.
31. Beachy, M. D.; Chasman, D.; Murphy, R. B.; Halgren, T. A.; Friesner, R. A. J Am Chem Soc 1997, 119, 5908–5920.
32. Krimm, S.; Bandekar, J. Adv Protein Chem 1986, 38, 181–364.
33. Bour, P.; Keiderling, T. A. J Am Chem Soc 1993, 115, 9602–9607.
34. Kubelka, J.; Silva, R. A. G. D.; Bour, P.; Decatur, S. M.; Keiderling, T. A. In Chirality: Physical Chemistry; ACS Symp. Ser. 810; Hicks, J. M., Ed.; American Chemical Society: Washington DC, 2002; Vol 810, pp 50–64.
35. Perczel, A.; Farkas, O.; Marcoccia, J. F.; Csizmadia, I. G. Int. J. Quant Chem 1997, 61, 797–814.
36. Csaszar, A. G.; Perczel, A. Progr Biophys Mol Biol 1999, 71, 243–309.
37. Challacombe, M.; Schwegler, E. J Chem Phys 1996, 106, 5526–5535.
38. Strain, M. C.; Scuseria, G. E.; Frisch, M. J. Science 1996, 271, 51–53.
39. Scusseria, G. J Phys Chem A 1999, 103, 4782–4790.
40. Van Alsenoy, C.; Yu, C.-H.; Peeters, A.; Martin, J. M. L.; Schafer, L. J Phys Chem A 1998, 102, 2246–2251.
41. Bour, P.; Sopkova, J.; Bednarova, L.; Malon, P.; Keiderling, T. A. J Comp Chem 1997, 18, 646–659.
42. Bour, P.; Kubelka, J.; Keiderling, T. A. Biopolymers 2000, 53, 380–395.
43. Klamt, A.; Schuurmann, G. J Chem Soc Perkin Trans 1993, 2, 799–805.
44. Kubelka, J.; Keiderling, T. A. J Am Chem Soc 2001, 123, 12048–12058.
45. Kubelka, J.; Keiderling, T. A. J Am Chem Soc 2001, 123, 6142–6150.
46. Hilario, J.; Kubelka, J.; Syud, F. A.; Gellman, S. H.; Keiderling, T. A. Biopolymers (Biospectroscopy) 2002, 67, 233–263.
47. Ahlrichs, R.; Bar, M.; Baron, H.-P.; Bauernschmitt, R.; Bocker, S.; Ehrig, M.; Eichkorn, K.; Elliot, S.; Furche, F.; Haase, F.; Haser, M.; Horn, H.; Huber, C.; Huniar, U.; Kattannek, M.; Kolmel, C.; Koolwitz, M.; May, K.; Ochsenfeld, C.; Ohm, H.; Schafer, A.; Schneider, U.; Treutler, O.; von Arnim, M.; Weigend, F.; Weis, P.; Weiss, H., Eds. Turbomole, version 5; Quantum Chemistry Group, University of Karlsruhe: Karlsruhe, 1998.
48. Creighton, T. E. Proteins: Structures and Molecular Properties; 2nd ed.; W. H. Freeman: New York, 1993.
49. Becke, A. D. J Chem Phys 1993, 98, 5648–5652.
50. Stephens, P. J. J Phys Chem 1985, 89, 748–752.
51. Cheeseman, J. R.; Frisch, M. J.; Devlin, F. J.; Stephens, P. J Chem Phys Lett 1996, 252, 211–220.
52. Frisch, M. J.; Trucks, G. W.; Schlegel, H. B.; Scuseria, G. E.; Robb, M. A.; Cheeseman, J. R.; Zakrzewski, V. G.; Montgomery, J., J. A.; Stratmann, R. E.; Burant, J. C.; Dapprich, S.; Millam, J. M.; Daniels, A. D.; Kudin, K. N.; Strain, M. C.; Farkas, O.; Tomasi, J.; Barone, V.; Cossi, M.; Cammi, R.; Mennucci, B.; Pomelli, C.; Adamo, C.; Clifford, S.; Ochterski, J.; Petersson, G. A.; Ayala, P. Y.; Cui, Q.; Morokuma, K.; Malick, D. K.; Rabuck, A. D.; Raghavachari, K.; Foresman, J. B.; Cioslowski, J.; Ortiz, J. V.; Stefanov, B. B.; Liu, G.; Liashenko, A.; Piskorz, P.; Komaromi, I.; Gomperts, R.; Martin, R. L.; Fox, D. J.; Keith, T.; Al-Laham, M. A.; Peng, C. Y.; Nanayakkara, A.; Gonzalez, C.; Challacombe, M.; Gill, P. M. W.; Johnson, B.; Chen, W.; Wong, M. W.; Andres, J. L.; Gonzalez, C.; Head-Gordon, M.; Replogle, E. S.; Pople, J. A., Eds. Gaussian 98; Revision A.6 ed.; Gaussian: Pittsburgh, PA, 1998.
53. Becke, A. Phys Rev A 1988, 38, 3098–3100.
54. Perdew, J. P.; Wang, Y. Phys Rev B 1992, 45, 13244–13249.
55. Kubelka, J.; Silva, R. A. G. D.; Keiderling, T. A. J Am Chem Soc 2002, 124, 5325–5332.
56. Kubelka, J. PhD. thesis, University of Illinois at Chicago, 2002.
57. Polese, A.; Formaggio, F.; Crisma, M.; Valle, G.; Toniolo, C.; Bonora, G. M.; Broxterman, Q. B.; Kamphuis, J. Chem A Eur J 1996, 2, 1104–1111.
58. Prasad, B. V. V.; Sasisekharan, V. Macromolecules 1979, 12, 1107–1110.
59. Dwivedi, A. M.; Krimm, S.; Malcolm, B. R. Biopolymers 1984, 23, 2025–2065.
60. Nemethy, G.; Phillips, D. C.; Leach, S. J.; Sheraga, H. A. Nature (London) 1967, 214, 363–365.
61. Fraser, R. D. B.; McRae, T. P. Conformation in Fibrous Proteins; Academic Press: New York, 1973.
62. Vaney, M. C.; Maignan, S.; Rieskautt, M.; Ducruix, A. Acta Crystallogr Sect D: Biol Crystalogr 1996, 52, 505–517.
63. Mahoney, N. M.; Janmey, P. A.; Almo, C. S. Nature Struct Biol 1997, 4, 953–960.
64. Dwivedi, A. M.; Krimm, S. Biopolymers 1982, 21, 2377–2397.
65. Kubelka, J.; Keiderling, T. A. J Phys Chem A 2001, 105, 10922–10928.
66. Dukor, R. K.; Keiderling, T. A. Biospectroscopy 1996, 2, 83–100.
67. Dukor, R. K.; Keiderling, T. A.; Gut, V. Int J Pept Protein Res 1991, 38, 198–203.
68. Dukor, R. K. PhD thesis, University of Illinois at Chicago, 1991.

69. Martin, J. M. L. In Encyclopedia of Computational Chemistry; Schleyer, v. R., Ed.; Wiley: Chichester, 1998; Vol 1, pp 115–128.
70. Huston, S. E.; Marshall, G. R. Biopolymers 1994, 34, 75–90.
71. Tirado-Rives, J.; Maxwell, D. S.; Jorgensen, W. L. J Am Chem Soc 1993, 115, 11590–11593.
72. Zhang, L.; Hermans, J. J Am Chem Soc 1994, 116, 11915–11921.
73. Young, W. S.; Brooks, C. L., III. J Mol Biol 1996, 259, 560–572.
74. Mandelkern, L. In Poly-α-Amino Acids; Fasman, G. D., Ed.; Dekker: New York, 1967.
75. Fasman, G. D. Prediction of Protein Structure and the Principles of Protein Conformation; Plenum: New York, 1989.
76. Hol, W. G. J. Progr Biophys Mol Biol 1985, 45, 149–195.
77. Parthasarathy, R.; Chaturvedi, S.; Go, K. Progr Biophys Mol Biol 1995, 64, 1–54.
78. Aurora, R.; Rose, G. D. Protein Sci 1998, 7, 21–38.
79. Penel, S.; Hughes, E.; Doig, A. J. J Mol Biol 1999, 287, 127–143.
80. Malon, P.; Kobrinskaya, R.; Keiderling, T. A. Biopolymers 1988, 27, 733–746.